CMOS-COMPATIBLE 2-AXIS SELF-ALIGNED VERTICAL COMB-DRIVEN MICROMIRROR FOR LARGE FIELD-OF-VIEW MICROENDOSCOPES

K. Kumar, and X.J. Zhang
Department of Biomedical Engineering, University of Texas at Austin, TX, USA

ABSTRACT

A CMOS-compatible 3-mask process for 2-axis self-aligned vertical comb-driven micromirror fabrication is described. Our 1024μm diameter mirrors exhibit resonance at 2.81kHz, 669Hz, and maximum scan angles of 22°, 12° and 5.0°, 4.5° for resonant and static voltage operation on inner and outer axes. Reflectance confocal images of USAF1951 resolution target and epithelial breast tissue obtained at 3.0fps with 0.49μm, 4.18μm lateral and axial resolution over 200×125μm field of view indicate the potential of these devices for large field-of-view microendoscopes.

INTRODUCTION

Fast-scanning micromirrors are an enabling technology for numerous applications including optical communication switching [1], display [2], and point-by-point image acquisition systems [3-5]. Of particular interest is the ability to integrate such micromirrors into compact laser-scanning micro-endoscopes. *In vivo* microendoscopy is an important tool for biopsy-free disease diagnosis, guided precision surgery, and minimally invasive assessment of the treatment [6]. This miniaturized instrumentation can greatly improve patient prognosis, especially in time-critical applications (such as staging of tumors), while reducing screening costs, treatment delay, and occurrences of unnecessary and potentially harmful treatment.

Current endoscopic approaches to beam deflection across the sample usually involve sideways-imaging proximal scanning techniques, wherein a fiber-fused graded-index lens and micro-prism assembly is rotated and/or translated within a protective sheath to obtain 2D or 3D images [7, 8]. Although such techniques provide reduced form factor, their scans are slow, exhibits poor repeatability, and are useful only in tubular human organs such as the esophagus or gastrointestinal tract. Forward-imaging techniques are better suited to imaging in non-tubular organs, but have been difficult to miniaturize thus far. A fiber-optic bundle of closely-spaced single-mode fibers packaged with an objective lens has been used for *in vivo* imaging by directing illumination through each fiber sequentially [9]. Though compact, this method suffers from pixilation artifacts in imaging and low spatial resolution due to finite fiber core spacing. Microelectromechanical system (MEMS) technologies offer the unique capability to package micro-optical elements with actuators at the distal end for *in vivo* imaging. Distal scanning has been achieved by fiber/objective translation [10, 11], or by micromirror-based angular beam deflection [3-5]. Electrostatic [10] and piezoelectric [11] actuators have been used to translate the fiber or objective lens. These techniques suffer from slow scan rates and the field-of-view is limited either by demagnification of the objective lens or optical aberrations.

Micromirrors actuated in one and two dimensions by parallel-plate and vertical comb drives have been used in optical coherence tomography [5], and confocal [3] and multi-photon microscopy [4]. Both angular [12] and staggered [13] vertical comb-driven micromirrors have been shown to be useful for building forward-imaging probes, providing large actuation torque and scanning angles with smooth optical surfaces and low dynamic mirror deformation. Unfortunately, these micromirrors do not offer perfectly linear transformation between input voltage and mechanical scan angle, and can often experience scanning instabilities due to pull-in phenomena. Complicated comb self-alignment procedures have therefore been adopted in scanner microfabrication to mitigate this problem. The present research attempts to addresses these drawbacks by introducing a simple 3-mask comb self-aligned micromirror fabrication process compatible with traditional CMOS processing in the semiconductor industry. The trend of merging standard COMS process and special post-CMOS processes with MEMS have been summarized [14]. The major advantage is the monolithic integration of the IC and MEMS components toward multifunctional and intelligent microsystems. Our process only utilizes conventional silicon processing tools which operate at temperatures low enough to allow pre-fabrication of CMOS circuitry on the wafer prior to commencing micromirror fabrication. For microendoscopes, this can enable CMOS-MEMS integration [14, 15] of control electronics and sensors to adaptively correct for aberrations in beam scanning along with power amplifier drive electronics, while significantly reducing fabrication costs and lowering the barriers towards clinical applications .

FABRICATION PROCESS

The micromirror fabrication process is shown in Figure 1. Double SOI wafers, having device and buried oxide layers of thickness 30μm and 1μm respectively, serve as the starting material. Silicon dioxide (LTO) is deposited by low-temperature chemical vapor deposition to create a hard etch mask. Coarse features (mask 1) of micromirror stator structures are etched into the LTO by reactive ion etching (RIE). Photolithography of exact micromirror features (mask 2) is performed, aligned to the coarse features in LTO. Self-alignment of the rotor comb structures to the stator occurs during this alignment process. The misalignment tolerance for this lithography step is half the comb gap spacing. Since the alignment procedure is extremely simple, the minimum comb spacing is determined solely by the aspect ratio achievable by the silicon deep reactive ion etching steps following creation of the mask. Oxide RIE to remove exposed silicon dioxide completes hard mask formation. The photoresist remaining after oxide RIE is not removed and, in combination with the underlying silicon dioxide, forms the mask for deep etching. Deep reactive ion etching (DRIE), stopped on the first buried oxide layer, creates features of both stator and rotor combs in the upper device

978-1-4244-2978-3/09/$25.00 ©2009 IEEE

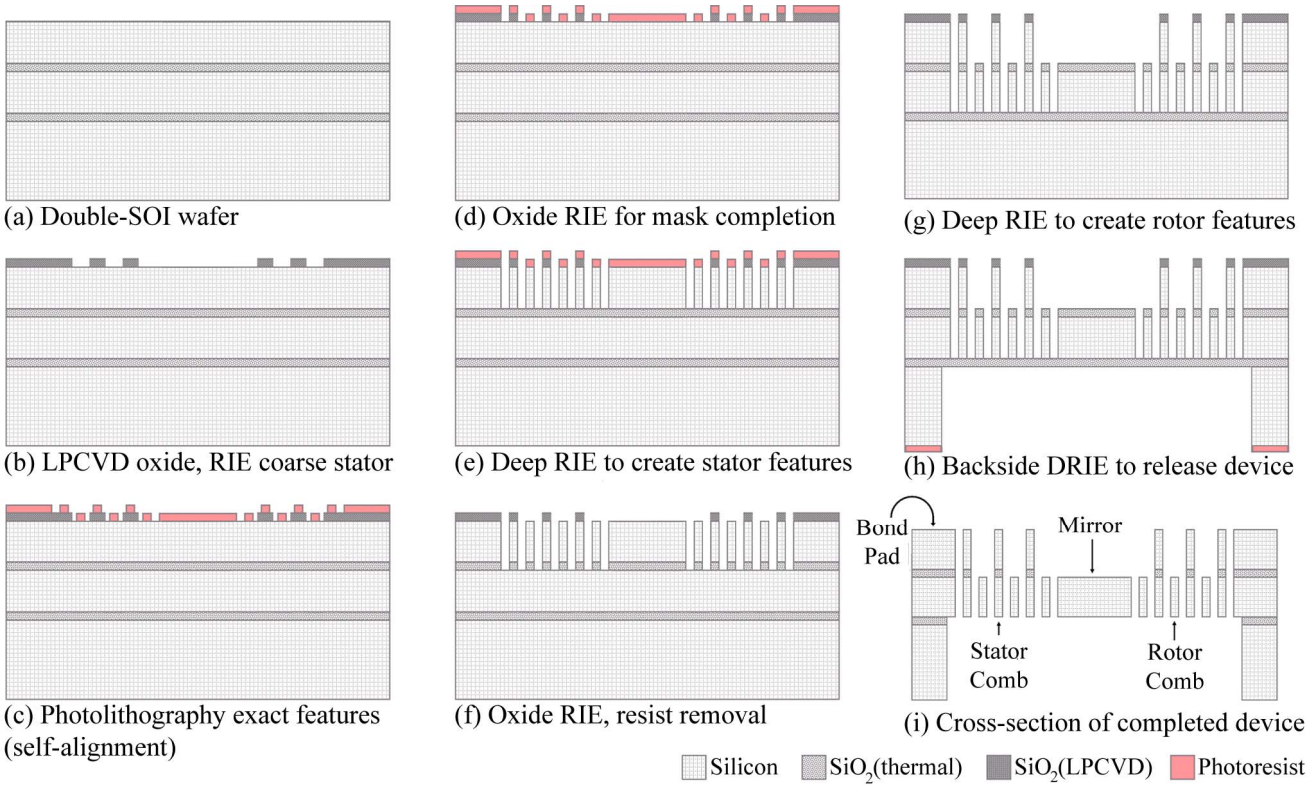

Figure 1: CMOS-compatible fabrication process for 2-axis self-aligned vertical comb-driven micromirror

layer. After RIE of the first intermediate buried oxide layer the photoresist component of the mask is removed, leaving the rotor features in the upper device layer unprotected by any masking element, while the stator features are still protected by a layer of LTO (Figure 1(f)). A second DRIE etch stopped on the second buried oxide layer removes the upper device layer silicon above the rotor combs while simultaneously defining the rotor features in the lower device layer. After etch completion, rotor layer features reside only in the lower layer of device silicon, while the stator layer extends through both device layers. The lower section of the stator features is redundant from an actuation perspective, but does not affect micromirror operation. Backside substrate DRIE (mask 3) followed by oxide RIE on front and back sides to remove any remaining oxide in the mask and second buried oxide layers releases the device and completes the fabrication process.

DEVICE CHARACTERIZATION

For initial experiments, we fabricated micromirrors with 1024µm diameter on wafers without pre-fabricated CMOS circuitry. Each micromirror was actuated by two sets of combdrive actuators for each rotation axis (Figure 2). Comb finger thickness and spacing between rotor and stator combs was fixed at 8µm, and the distance between rotor tip and central axis of rotation was maintained at 200µm or 250µm. Chip size is 2.8mm^2.

A critical requirement of the fabrication process is to ensure optically smooth mirror surface in the completed device. We measured the mirror surface roughness using a Zygo white-light interferometry-based 3D surface profiler

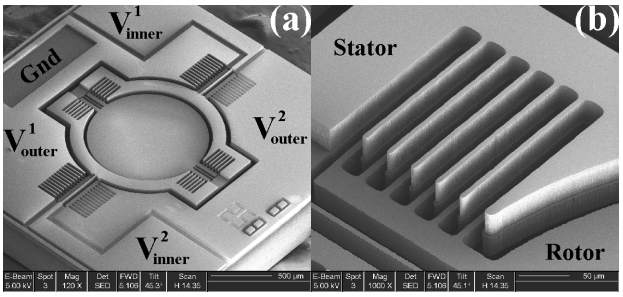

Figure 2: Scanning electron micrographs of fabricated device. (a) Oblique view showing mirror, combdrives, and electrical bond pads. (b) Close-in view of vertical combdrive actuators arrangement.

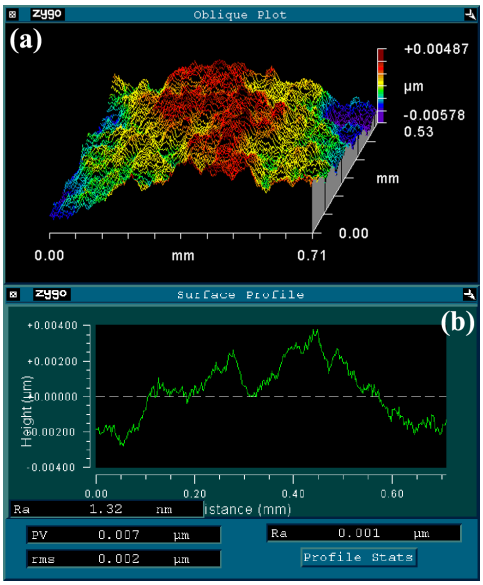

Figure 3: Sample mirror surface roughness measurement by white-light interferometry 3D surface profiler. (a) 2D map of surface roughness over 700×500µm area. (b) 1D slice plot of surface profile across mirror.

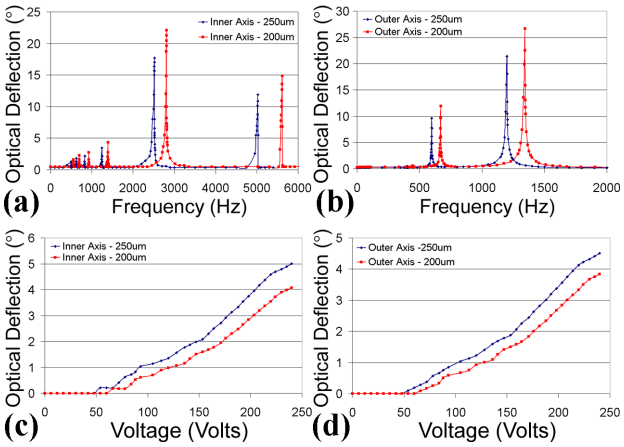

Figure 4: Operating curves for devices having rotor tip-axis separation of 200/250μm. (a)-(b) Frequency response of inner and outer axes. (c)-(d) Static voltage characteristic (using 1 comb set) of inner and outer axes.

to be 8nm RMS on average (Figure 3).

Micromirror operating characteristics are depicted in Figure 4. The devices exhibit primary resonances (ω_0) around 2.81kHz and 670Hz, with optical scan angles of 22° and 12° on inner and outer axes respectively. Secondary resonances are observed at $2\omega_0$ and $\omega_0/2$, $\omega_0/3$, $\omega_0/4$ etc., as reported previously for micromirrors of similar configuration [16]. Scan angles of 5° and 4.5° for inner and outer axes respectively are observed on applying up to 240V of static voltage to one comb of each rotation axis. Raster scan pattern for imaging is achieved by operating the inner axis on resonance (using one inner comb bank) while actuating the outer axis using both comb banks at low frequency in non-resonant mode. Reducing the comb gap spacing and optimizing comb finger length will reduce operating voltages required to achieve a specified scan angle, while also matching the voltage dynamic range of the high voltage amplifier with the maximum scan angle of the micromirror.

IMAGING EXPERIMENTS

The devices were incorporated into a laser-scanning reflectance confocal microscope instrument, depicted in Figure 5. Linearly polarized light from a 635nm diode laser is coupled into a single-mode polarization maintaining (PM) fiber. Light exiting the fiber is collimated to 1mm beam diameter through a zero-order quarter wave-plate whose axis is oriented at 45° to the incident polarization angle, converting the illumination to circular polarization. After reflection off a stationary mirror, the illumination is incident on the micromirror at

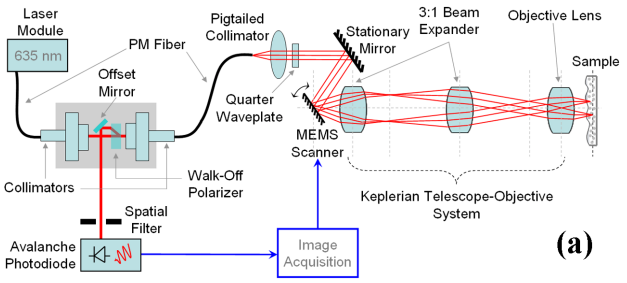

Figure 5: CMOS-MEMS micromirror-based laser scanning confocal microscope instrumentation set-up.

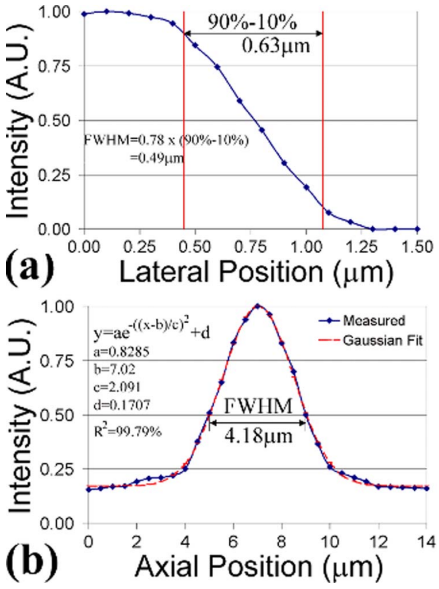

Figure 6: Experimental measurements of (a) Lateral and (b) Axial resolution of MEMS-based reflectance confocal microscope instrument.

22.5° to the micromirror normal. The micromirror scans the illumination across an objective system consisting of a 3X Keplerian beam expander and a high-NA aspheric objective lens, providing effective numerical aperture of 0.48 at the sample. Reflected light is converted into linear polarization orthogonal to the initial illumination polarization, isolated using a walk-off polarizer and offset mirror, and directed through a spatial filter into an avalanche photodetector. Image acquisition is performed through a National Instruments PCI-6111 card controlled by Matlab® software. Experimental measurements of resolution (Figure 6) by translating a mirror edge laterally across the beam spot in the focal plane, and a mirror

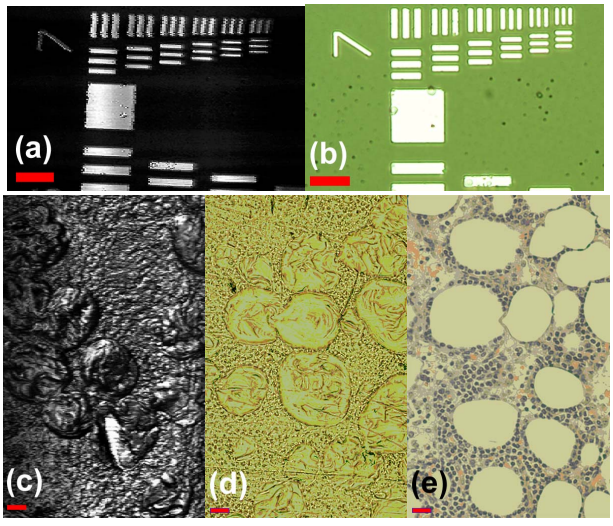

Figure 7: Imaging results. (a) USAF1951 target group 7. (b) Comparison image from Olympus BX51 microscope (20X, reflectance). (c). Human epithelial breast tissue (4 fields stitched). (d) Comparison image from Olympus BX51 microscope (20X, bright-field) (e) Image of H/E stained slice of epithelial breast tissue sectioned from just above slice used in (d) using Olympus BX51 microscope (20X, bright-field). Field of view (unstitched images) is 200×125μm. Scale bar: 25μm.

axially through the focal plane showed that lateral and axial resolutions of the system are 0.49µm and 4.18µm respectively, which is comparable with conventional histology.

The instrument provided images of a 200×125µm field of view at 3.0 frames per second. The number of resolvable points in the images (408×255), which is proportional to the product of mirror diameter and optical scan angle, is a 4X improvement over previous results for similar micromirrors. Images of the elements of group 7 of a standard USAF 1951 resolution target are depicted in Figure 7(a), compared against an image acquired by an Olympus BX51 bright-field microscope with a 20X objective. The smallest lines in group 7 are of 2.2µm width. We also obtained images of fixed human epithelial breast tissue without use of contrast agents. The result of stitching four such fields together (Figure 7(c)) is compared against bright-field images using an Olympus BX51microscope with 20X objective of the unstained slice, and the slice stained with hematoxylin/eosin stain used for conventional histology.

CONCLUSIONS

A simple 3-mask CMOS-compatible process for 2-axis self-aligned vertical comb-driven micromirror fabrication is demonstrated. Reflectance confocal imaging using the device is shown with resolution comparable to conventional histology, and 4X improvement in number of resolvable points per image over previous micromirrors of similar configuration. Minimization of comb gap spacing can reduce operating voltages required. The monolithically integrated CMOS-MEMS design further enables pre-fabrication of control electronics and sensors for adaptive beam scan control, and power amplifier drive electronics in compact form suitable for next generation microendoscopes.

ACKNOWLEDGEMENT

The authors gratefully acknowledge financial support for this research from the Wallace H Coulter Foundation Early Career Award 2006–08. The micromirrors were fabricated at Stanford Nanofabrication Facility (supported by National Science Foundation grant no. 9731293) and University of Texas–Austin Microelectronics Research Center (supported by National Science Foundation grant no. 0335765) under the National Nanofabrication Infrastructure Network. Epithelial breast tissue samples were provided by Prof. Tse-Kuan Yu, Department of Radiation Oncology, University of Texas M.D. Anderson Cancer Center, Houston, TX.

REFERENCES

[1] S.-S. Lee, L.-S. Huang, C.-J. Kim, and M. C. Wu, "Free-Space Fiber-Optic Switches Based on MEMS Vertical Torsion Mirrors," *J. Lightwave Technol.*, vol. 17, pp. 7, 1999.

[2] J. Yan, S. T. Kowel, H. J. Cho, and C. H. Ahn, "Real-time full-color three-dimensional display with a micromirror array," *Optics Letters*, vol. 26, pp. 1075-1077, 2001.

[3] K. Kumar, K. Hoshino, and X. Zhang, "Handheld subcellular-resolution single-fiber confocal microscope using high-reflectivity two-axis vertical combdrive silicon microscanner," *Biomedical Microdevices*, vol. 10, pp. 653-660, 2008.

[4] W. Piyawattanametha, R. P. J. Barretto, T. H. Ko, B. A. Flusberg, E. D. Cocker, H. Ra, D. Lee, O. Solgaard, and M. J. Schnitzer, "Fast-scanning two-photon fluorescence imaging based on a microelectromechanical systems two- dimensional scanning mirror," *Opt. Lett.*, vol. 31, pp. 2018-2020, 2006.

[5] T. Xie, H. Xie, G. K. Fedder, and Y. Pan, "Endoscopic optical coherence tomography with a modified microelectromechanical systems mirror for detection of bladder cancers," *Applied Optics*, vol. 42, pp. 6422-6426, 2003.

[6] Z. Yaqoob, J. Wu, E. J. McDowell, X. Heng, and C. Yang, "Methods and application areas of endoscopic optical coherence tomography," *Journal of Biomedical Optics*, vol. 11, pp. 063001, 2006.

[7] J. Su, J. Zhang, L. Yu, and Z. Chen, "In vivo three-dimensional microelectromechanical endoscopic swept source optical coherence tomography," *Opt. Express*, vol. 15, pp. 10390-10396, 2007.

[8] P. H. Tran, D. S. Mukai, M. Brenner, and Z. Chen, "In vivo endoscopic optical coherence tomography by use of a rotational microelectromechanical system probe," *Opt. Lett.*, vol. 29, pp. 1236-1238, 2004.

[9] A. F. Gmitro and D. Aziz, "Confocal microscopy through a fiber-optic imaging bundle," *Opt. Lett.*, vol. 18, pp. 565, 1993.

[10] S. Kwon and L. P. Lee, "Micromachined transmissive scanning confocal microscope," *Optics Letters*, vol. 29, pp. 706-708, 2004.

[11] S. A. Boppart, B. E. Bouma, C. Pitris, G. J. Tearney, and J. G. Fujimoto, "Forward-imaging instruments for optical coherence tomography," *Optics Letters*, vol. 22, pp. 1618-1620, 1997.

[12] D. Hah, P. R. Patterson, H. D. Nguyen, H. Toshiyoshi, and M. C. Wu, "Theory and Experiments of Angular Vertical Comb-Drive Actuators for Scanning Micromirrors," *IEEE Journal of Selected Topics in Quantum Electronics*, vol. 10, pp. 505-513, 2004.

[13] C. Hyuck, D. Garmire, J. Demmel, and R. S. Muller, "Simple Fabrication Process for Self-Aligned, High-Performance Microscanners— Demonstrated Use to Generate a 2-D Ablation Pattern," *Microelectromechanical Systems, Journal of*, vol. 16, pp. 260-268, 2007.

[14] G. K. Fedder, R. T. Howe, L. Tsu-Jae King, and E. P. Quevy, "Technologies for Cofabricating MEMS and Electronics," *Proceedings of the IEEE*, vol. 96, pp. 306-322, 2008.

[15] C.-L. Dai, F.-Y. Xiao, Y.-Z. Juang, and C.-F. Chiu, "An approach to fabricating microstructures that incorporate circuits using a post-CMOS process," *Journal of Micromechanics and Microengineering*, vol. 15, pp. 98-103, 2005.

[16] D. Lee, "Design and fabrication of SOI-based micromirrors for optical applications," *Ph.D. Dissertation, Stanford University*, 2007.